



Axisymmetric squirmers in Stokes fluid with nonuniform viscosityPatrick S. Eastham ^{1,*} and Kourosh Shoele ²¹*Department of Mathematics, Florida State University, Tallahassee, Florida 32304, USA*²*Department of Mechanical Engineering, Florida State University–Florida A&M University, Tallahassee, Florida 32310, USA*

(Received 6 September 2019; accepted 28 April 2020; published 24 June 2020)

The ciliary locomotion and feeding of an axisymmetric microswimmer in a complex fluid whose viscosity depends on a surrounding nutrient field are investigated numerically in order to extend previous asymptotic results for weak nutrient-viscosity coupling. Numerical simulations capture nonlinearities inherent in the full system that are missed using perturbation-based linearization methods. The microswimmer's ciliary beating is modeled by a slip velocity, i.e., the squirmer model, and body geometry is modeled by spheroids. It is found that swimming speed and feeding are most affected by a nonuniform viscosity environment when the ratio of advection forces to diffusion transport, characterized by the nondimensional Peclét number, is moderate, i.e., $Pe = O(5)$. These changes are correlated to significant increases in the pressure force on the surface of the squirmer, as well as differences in power expenditure and hydrodynamic efficiency compared to the constant-viscosity case. Additionally, the swimming and feeding changes are found to be more significant in oblate spheroids than prolate spheroids, although the shape has a smaller effect on performance than Peclét number or surface stroke. These results suggest that nonlocal effects from viscosity variation are caused by a modification to the pressure force, as opposed to the strain rate. These results should be useful in interpreting experiments where a microswimmer affects a fluid's local rheology.

DOI: [10.1103/PhysRevFluids.5.063102](https://doi.org/10.1103/PhysRevFluids.5.063102)**I. INTRODUCTION**

Studying the locomotion principles of micrometer-scale organisms—commonly called microswimmers—inspires both biologists and engineers who wish to develop artificial microrobots for numerous applications such as targeted drug delivery [1–4] and miniature noninvasive surgery [5,6]. Through the evolutionary goals of colonization and efficient nutrient acquisition, many microorganisms adopt a specific means of swimming. Microswimmers such as bacteria, protozoa, and algae use appendages to move through their environment. These appendages can be categorized into two groups based on their morphology. The first group, flagella, are long, slender appendages typically present in small numbers on a cell surface. The second group, cilia, are shorter relative to swimmer size and often exist in groups of thousands. Ciliary swimmers in particular have been influential in the design of microrobots [7–13] and therefore will be the focus of this study.

Microswimmers commonly swim through complex fluids containing inhomogeneities that correspond to spatial variation in material properties. Aggregate suspensions of bacteria can affect a fluid's bulk viscosity [14–16] and, furthermore, some microswimmers may use spatial variations in viscosity to improve their locomotion [17,18]. In addition to swimming through complex environments, microswimmers can actively affect their surroundings. For bacteria, this is done

*Corresponding author: peastham@math.fsu.edu

through feeding on surrounding nutrients or other metabolic activity; for microrobots, this is done through surface heat dissipation or chemical reaction as a by-product of swimming actuation. These mechanisms have the theoretical potential to alter the local material properties of the surrounding fluid. This raises the question of whether it is possible for a swimmer to modify local fluid rheology in order to enhance its locomotion. In the case of bacteria, this could further be coupled to increased feeding rates, which would provide an obvious evolutionary advantage. Additionally, experimental exploration of the role of a fluid's microrheology on swimming performance is an active area of research [19,20], and the analysis presented here will aid in the interpretation of experimental results. The question considered in this paper is how a single microswimmer can actively modify local fluid properties in order to improve its locomotion or feeding performance.

The possibility for the existence of an active mechanism to improve locomotion or feeding is motivated by several biological examples. First, the microswimmer *H. pylori* modifies the properties of the surrounding fluid during its locomotion. This bacteria lives in the human stomach and uses enzymes to locally transform impenetrable stomach mucus into a softer material in which the organism has greater motility [21]. This modification of the environment by the microorganism has an important impact on the virulence of *H. pylori*, which by recent estimates has infected 50% of the world's population [22]. The microorganisms *Spiroplasma* [23] and *Leptospira interrogans* [24] have similarly demonstrated viscotaxis, although it is unclear if the organisms have any active role in affecting near-field viscosity. Another example is the multicellular *Volvox*. This algae could have a large rate of nutrient uptake and waste disposal and lives in a high-Peclet-number flow regime [25–27] where the nutrient field exhibits a flow-induced asymmetry near the body. Colonies of *Volvox* also exhibit enhanced mixing with a non-Gaussian distribution of tracer displacement [28,29]. The question is whether nutrient-dependent flow characteristics and induced material non-linearity can influence the flow statistics near the body and contribute to the deviation from Gaussian statistics in this system. It might also constructively influence the rotational steering observed in *Volvox carteri* [30,31] and *C. crescentus* [32].

In addition to these biological motivations, the coupling between transport of scalar fields (e.g., nutrients, temperature, and chemicals) and flow dynamics could be leveraged to manufacture more efficient swimming microrobots. In general, two modes of swimming are available: passive and active. Inert particles generate thrust passively through the use of gradients in a surrounding scalar field. These gradients generate a slip velocity on the surface of the particle that results in phoretic propulsion [33–35]. For an active swimmer, the surface slip velocity is generated by the particle itself (e.g., bacteria and microrobots). Whether an active swimmer can benefit from the passive mechanisms of well-coordinated scalar transport is an open question. This paper seeks to address this question by considering a combination of passive and active effects; the squirmer is an active swimmer whose cilia produce a slip velocity on the surface, but the dependence of the fluid viscosity on the surrounding nutrient concentration allows a feedback mechanism for the stroke motion to induce passive phoretic propulsion.

When a fluid environment is modeled by linear, constant-coefficient PDEs, as is the case in constant-viscosity Stokes equation, one can employ classical techniques to find fundamental solutions of the flow field produced by ciliary beating. This approach has been successfully applied to ciliary microswimmers in Newtonian fluids [36–41]. More recently, there has been an interest in understanding how the swimming performance of microswimmers changes in a complex fluid environment with nonlinear rheology. This is motivated by the fact that real-world fluid environments contain numerous complexities such as particles, polymers, and temperature [42]. As stated above, spatial gradients in these complexities can induce local modification to the fluid rheology and consequently affect the governing constitutive relation between stress and shear rate; unfortunately, these complexities also reduce the number of analytic solutions available.

Governing flow equations that are only *weakly* nonlinear can be solved with asymptotic techniques. These techniques can be accompanied by the powerful generalized reciprocal theorem (GRT) [43] to explain swimming performance changes [44–46]. The GRT—where a known auxiliary solution is employed to solve for quantities, such as swimming speed, in a corresponding

domain—has been used to study the effect of weakly nonlinear shear-thinning viscosity [47,48] and viscoelasticity [49–52] on microswimmer mobility. This technique was used previously by the authors to show that, when the fluid viscosity depends *weakly* on nutrient concentration, the optimal swimming speed of the constant-viscosity microswimmer can further increase, among other results [53]. This suggests that a microorganism could harness the viscosity-modifying properties of nutrient concentration to swim faster. However, since the effect of variable viscosity on feeding occurs at higher order asymptotic terms than examined, investigating the effect of nutrient-dependent viscosity on nutrient uptake requires different methods.

To study systems with substantial nonlinearity, e.g., resulting from a strong nutrient-viscosity coupling, one often requires numerical methods. To solve the problem considered here—a coupled variable-coefficient Stokes and advection-diffusion system—the finite element method is employed. The generality of this method allows us to examine complex domains that would be difficult to achieve with other methods such as finite differences [54]. Although boundary integral methods have been employed to study ciliated swimmers [55,56], the presence of variable coefficients in our problem undermines their computational efficiency. The canonical model of a spheroidal squirmer allows us to explore the feedback mechanisms between passive and active swimming methods in a computationally efficient manner.

The paper proceeds as follows: Section II describes the squirmer model, first in general and then using specific conditions for our simulations and its numerical discretization. Section III contains descriptions of the results for different parameter regimes, including the effect of Peclét number, strength and type of nutrient-viscosity (and nutrient-diffusivity) relationship, squirmer surface motion, and squirmer geometry. Section IV concludes by discussing the importance and significance of our findings in the wider context of the microswimmer and complex fluids community.

II. SCALAR TRANSPORT AROUND AN AXISYMMETRIC SQUIRMER

We consider a spheroidal squirmer with surface \mathcal{S} in an unbounded domain \mathcal{D} at negligible Reynolds number $\text{Re} = \rho U \alpha / \mu_0 \ll 1$, where ρ is the constant fluid mass density, U is the characteristic swimming velocity, α is the characteristic length of the squirmer, and μ_0 is the characteristic (far-field) viscosity of the fluid. We additionally assume that ciliary beating (with frequency σ) is slow enough that $\sigma \text{Re} \ll 1$ and therefore the steady approximation is valid. The axisymmetric squirmer model in a spatially varying nutrient field is described in a general form in Sec. II A. In Sec. II B, we simplify this general model for our specific squirmer configuration as well as enforce additional constraints to assist physical interpretation of the results. We then detail our numerical discretization of the strongly coupled system by the finite-element method in Sec. II C.

A. General steady squirmer in a nutrient-dependent fluid

We follow the general model previously proposed by Magar *et al.* [57] and Michelin and Lauga [58], briefly restated here for convenience. More details can be found in Pedley [41] and Pak and Lauga [40]. In a body-fixed, axisymmetric coordinate system, the flow is governed by Stokes equations,

$$\nabla \cdot \mathbb{T} = \mathbf{0}, \quad \nabla \cdot \mathbf{u} = 0, \quad \text{for } \mathbf{x} \in \mathcal{D}, \quad (1a)$$

$$\mathbf{u} = \mathbf{u}^{\mathcal{S}}, \quad \text{for } \mathbf{x} \in \mathcal{S}, \quad (1b)$$

$$\mathbf{u} \rightarrow -\mathbf{U}, \quad \text{as } \|\mathbf{x}\| \rightarrow \infty, \quad (1c)$$

where \mathbf{u} is the fluid velocity, \mathbf{U} is the translational velocity of the squirmer, $\mathbb{T} = -p\mathbb{I} + 2\mu\mathbb{D}$ is the viscous stress tensor with spatially varying viscosity $\mu = \mu(\mathbf{x})$, p is the fluid pressure, $\mathbb{D}(\mathbf{u}) = \frac{1}{2}(\nabla\mathbf{u} + \nabla\mathbf{u}^{\top})$ is the strain rate tensor, and $\mathbf{u}^{\mathcal{S}}$ is the tangential squirmer motion on the surface \mathcal{S} with respect to the center of mass of the body.

The squirmer is assumed to be a free swimmer at zero Reynolds number where inertial effects are negligible. This implies the free-swimming condition which corresponds to zero drag on the body of the squirmer, $\int_S \boldsymbol{\tau} dS = \mathbf{0}$, where $\boldsymbol{\tau} = \mathbf{n} \cdot \mathbb{T}$ is the traction on the surface \mathcal{S} with \mathbf{n} being the unit normal vector pointing into the flow. Note that torque is always zero by the requirement of axisymmetry.

The characteristic length α is chosen to be the square root of the surface area of the squirmer, and characteristic velocity is $\sqrt{\mathcal{P}_0/\mu_0\alpha}$, where \mathcal{P}_0 is the power expenditure by an equivalent squirmer (with the same surface area) in a constant-viscosity fluid defined as

$$\mathcal{P} = \int_{\mathcal{D}} \mathbb{T} : \mathbb{D} dV = - \int_S \mathbf{u}^S \cdot \boldsymbol{\tau} dS. \quad (2)$$

This nondimensionalization is chosen so that comparisons can be made between different spheroidal geometries.

The scalar nutrient C is fully absorbed on the surface \mathcal{S} of the squirmer (i.e., ignoring metabolism) and approaches a limiting value of C_∞ in the far field. For convenience, the nutrient is normalized as $c = (C_\infty - C)/C_\infty$. In accordance with the Stokes-Einstein relationship, where diffusivity is inversely proportional to viscosity, we also assume variable diffusivity of the nutrient. The transport of c is modeled with an advection-diffusion equation in the body-fixed coordinate system:

$$\mathbf{u} \cdot \nabla c = \frac{1}{\text{Pe}} \nabla \cdot [H(c)\nabla c], \quad \text{for } \mathbf{x} \in \mathcal{D}, \quad (3a)$$

$$c = 1, \quad \text{for } \mathbf{x} \in \mathcal{S}, \quad (3b)$$

$$c \rightarrow 0, \quad \text{as } \|\mathbf{x}\| \rightarrow \infty, \quad (3c)$$

where

$$H(c) = 1 + k_\kappa c^\xi \quad (4)$$

is the nutrient-dependent diffusivity and the Peclet number is defined using the previously mentioned characteristic length and velocity, $\text{Pe} = \frac{1}{\kappa_0} \sqrt{\mathcal{P}_0\alpha/\mu_0}$, with κ_0 being the (constant) far-field nutrient diffusivity. Through a suitable rescaling, the normalized scalar field c can be interpreted as a different physical quantity, such as temperature or a chemical agent *emitted*, as opposed to absorbed, by the squirmer. Through Eq. (5), the viscosity depends on the nutrient field, and the nutrient field depends on the viscosity (through the velocity field), so a two-way coupling exists between Eqs. (1) and (3). To be clear, these governing equations assume that the spatiotemporal scales under consideration are large enough to neglect contributions from thermal or biological noise, effects that are sometimes considered when studying colloidal particles [59].

We follow our previous work in defining the pointwise dependence of viscosity [53] on nutrient in a canonical form as

$$\mu(c(\mathbf{x})) = \mu_0[1 + k_\mu c(\mathbf{x})^\xi], \quad (5)$$

where k_μ and ξ are parameters that govern the strength and qualitative nature of the relationship, respectively. The characteristic viscosity μ_0 corresponds to the viscosity of the nutrient-saturated fluid, i.e., the far field. Qualitatively, $k_\mu < 0$ corresponds to viscosity increasing with increasing nutrient C , as is the case with sugars, nitrate, and other complex proteins. Correspondingly, $k_\mu > 0$ means viscosity increases with decreasing C , for example, when C measures temperature or a different chemical whose presence decreases fluid viscosity [60–64]. In accordance with the Stokes-Einstein relationship, the strength of the nutrient-diffusivity relationship, k_κ , is typically the opposite sign of the nutrient-viscosity strength k_μ ; e.g., if viscosity increases with nutrient concentration, then diffusivity decreases. The power ξ is analogous to those used in power laws for shear-dependent viscosity flows, employed here to represent the potentially nonlinear relationship between nutrient concentration and viscosity or diffusivity. Figure 1 illustrates the qualitative

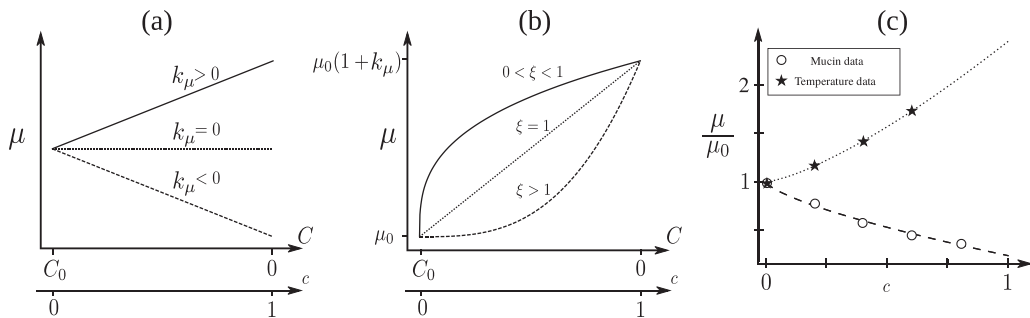


FIG. 1. The nutrient-viscosity relationship for (a) various k_μ , fixed $\xi = 1$, and (b) various ξ , fixed $k_\mu > 0$, and (c) fit to two real materials, using Eq. (5). Fitting the data for viscosity vs concentration of mucin, a protein, gives $k_\mu = -0.76$ and $\xi = 0.70$ [65]; fitting the data for viscosity vs water temperature gives $k_\mu = 1.45$ and $\xi = 1.35$ [66]. The power-law coefficient ξ determines the nonlinearity of relationship, while the magnitude and sign of k_μ determines the strength of the relationship and whether the viscosity increases or decreases near the surface of the squirmer ($C = 0, c = 1$), respectively. Note that C is the dimensional nutrient variable and c is its dimensionless counterpart.

behavior of μ with respect to nutrient in Eq. (5) and, in particular, Fig. 1(c) gives estimates for k_μ and ξ where C is Mucin concentration and water temperature from experimental viscosity data. These fit parameters motivate the need for both k_μ and ξ in Eq. (5).

Feeding by the microswimmer is modeled as the nutrient flux through the surface \mathcal{S} and is defined in its nondimensional form by

$$\Phi = -\frac{1}{\text{Pe}(1+k_\kappa)} \int_{\mathcal{S}} \frac{\partial c}{\partial n} dS, \quad (6)$$

where $\partial c/\partial n = \mathbf{n} \cdot \nabla c$. The coefficient in front of the integral differs from [58, Eq. (12)] due to the evaluation of the diffusivity function $H(c)$ on the swimmer surface, \mathcal{S} .

Finally, we note that the variable-viscosity Stokes problem in Eq. (1) with nutrient-dependent viscosity in Eq. (5) can be combined to generate the inhomogeneous Stokes problem

$$\nabla \tilde{p} + \nabla^2 \mathbf{u} = \mathcal{F}, \quad (7)$$

where $\tilde{p} = p/(\mu_0 k_\mu)$ and

$$\mathcal{F}(c, \mathbf{u}) = c^{\xi-1} [\nabla c (\nabla \mathbf{u} + \nabla \mathbf{u}^\top) - c \nabla^2 \mathbf{u}]. \quad (8)$$

This formulation indicates the “active force” exerted within a fluid with nutrient-dependent viscosity. This form of the fluid equation will aid our interpretation of results in Sec. III.

B. Spheroidal squirmer model

Spheroids are approximations for microswimmer geometries and are often used as a canonical representative shape [67,68]. Here, the squirmer surface \mathcal{S} is chosen to be a spheroid, also known as an axisymmetric ellipsoid, with principal semiaxes a, b , and c where $b = c$ provides axisymmetry along the swimming direction (see Fig. 2). The spheroid is characterized by the aspect ratio $\ell = a/b$, where for $\ell < 1, \ell = 1, \text{ or } \ell > 1$ the surface \mathcal{S} is called oblate, spherical, or prolate, respectively. As mentioned previously, to compare the swimming and feeding of various spheroids, the surface area of the swimmer, α^2 , is kept fixed for all aspect ratios ℓ . This constraint is motivated by the observation that both the power expenditure and feeding rate of a microswimmer during locomotion are proportional to the surface area.

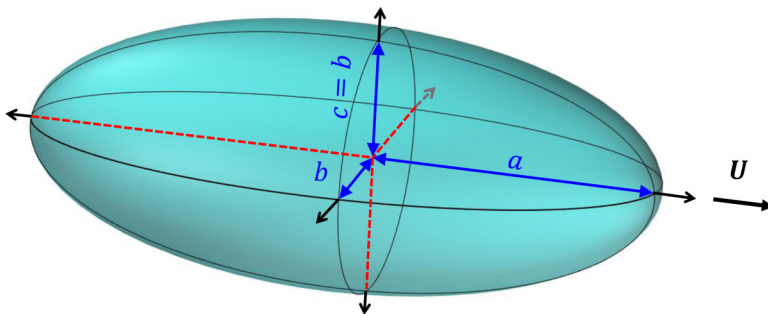


FIG. 2. Spheroidal microswimmer where $b = c$. The shape is prolate if $a > b$, spherical if $a = b$, and oblate if $a < b$.

The surface area α^2 can be approximately calculated based on the semiaxes of the spheroid according to

$$\alpha^2 = 4\pi \left(\frac{(ab)^p + (ac)^p + (bc)^p}{3} \right)^{1/p}, \quad (9)$$

where for $p = 1.6075$ the error of the surface area approximation is bounded by $\pm 1.061\%$ [69]. For a given aspect ratio ℓ and with the assumption that $b = c$, Eq. (9) is solved for b ,

$$b(\ell) = \left[\frac{3(\frac{\alpha^2}{4\pi})^p}{2\ell^p + 1} \right]^{1/(2p)}. \quad (10)$$

The surface motion \mathbf{u}^S consists of orthogonal, tangential “stroke modes” with the surface velocity of $\mathbf{u}^S = u_t^S \mathbf{e}_t$, where \mathbf{e}_t is the unit tangent vector on the surface of the spheroid. The surface velocity magnitude u_t^S is represented by

$$u_t^S(\gamma) = \sum_{n=1}^{\infty} \beta_n K_n(\gamma), \quad K_n(\gamma) = \sqrt{\frac{3}{n(n+1)}} \sqrt{1 - \gamma^2} P'_n(\gamma), \quad (11)$$

where for each orthogonal mode n , $P_n(\gamma)$ is the n th-order Legendre polynomial and $\gamma = \cos(2\pi\chi/L_E)$. Here, L_E is the total arclength of the ellipse with semiaxis a and b and χ is the arclength from the front point to a particular point on the surface. We note that \mathbf{u}^S is slightly modified from Shoele and Eastham [53], who considered only spheres, to adjust for arc length along the spheroid.

The surface stroke modes β_n are constrained by

$$\frac{2}{3}\beta_1^2 + \sum_{n=2}^{\infty} \beta_n^2 = 1, \quad (12)$$

which, in the constant-viscosity case, fixes the power expenditure of the squirmer as defined in Eq. (2). In the variable-viscosity case, however, the power is not fixed because the viscous stress is affected by the distribution of the scalar field c . In order to account for this variation, we will consider the low-Re hydrodynamic efficiency η , defined to be [70, Eq. (20)]

$$\eta = \frac{U \langle \mathcal{D} \rangle}{\langle \mathcal{P} \rangle}, \quad (13)$$

where $\langle \mathcal{D} \rangle$ is the average drag on an inert body traveling with speed U , and $\langle \mathcal{P} \rangle$ is the average power expended by the swimmer with surface actuation. In the case of steady governing equations, $\langle \mathcal{P} \rangle$ is given by Eq. (2).

This paper addresses the following question: What is the relative change in swimming and feeding performance for an axisymmetric squirmer in a fluid with a *strong* nutrient-viscosity (and nutrient-diffusivity) relationship? As the two-way coupling introduces a strong nonlinearity into our governing equations, answering this question requires numerical simulation. As we will show, these numerical simulations will allow us to address modifications in nutrient flux, hydrostatic pressure, power consumption, and hydrodynamic efficiency that are not present in a weak coupling.

C. Numerical methodology

We employ the finite-element method (FEM) [71,72] to numerically calculate the flow and nutrient fields around a free-swimming, steady squirmer. Simulations are done using an in-house FEM package developed in the JULIA programming language [73,74] and uses mesh data files generated in Gmsh, an open-source finite element mesh generator [75]. Flow field visualizations were done using VISIT [76], while contour and line plots were done in MATLAB [77].

We follow the derivation given by Tabata [78] for the axisymmetric Stokes equations and reformulate Eq. (1) into the following weak form:

$$\iint_{\mathcal{D}'} 2\mu \left[\mathbb{D}(\mathbf{u}) : \mathbb{D}(\mathbf{v}) + \frac{u_r v_r}{r^2} \right] r dr dx - \iint_{\mathcal{D}'} p(\nabla \cdot \mathbf{v}) r dr dx = 0, \quad (14a)$$

$$\iint_{\mathcal{D}'} q(\nabla \cdot \mathbf{u}) r dr dx = 0, \quad (14b)$$

for proper test functions q and $\mathbf{v} = v_x \hat{\mathbf{e}}_x + v_r \hat{\mathbf{e}}_r$, where \mathcal{D}' is a cross section through our three-dimensional (3D) domain along the axis of symmetry, and \mathbb{D} is defined after Eq. (1). Note that x is the axis of symmetry and $r \geq 0$ is the radial coordinate. The axisymmetric weak form of the advection-diffusion system is

$$\text{Pe} \iint_{\mathcal{D}'} \psi(\mathbf{u} \cdot \nabla c) r dr dx = \iint_{\mathcal{D}'} H(c)(\nabla c \cdot \nabla \psi) r dr dx, \quad (15)$$

where ψ is a test function. The flow solution (\mathbf{u}, p) is calculated using quadrilateral Q_2 - Q_1 Taylor-Hood elements and c is calculated using Q_2 elements.

The computational model is carefully validated for different canonical problems and closed-form solutions, including comparison to asymptotic results from Ref. [53] in Fig. 3. The velocity and scalar c converge with $O(h^{-4})$, consistent with Q_2 elements, and pressure converges with $O(h^{-2})$, consistent with Q_1 elements, where h is the characteristic edge length for the mesh. Based on the convergence study, the mesh resolution of approximately $h \approx 0.02$ was chosen near the squirmer surface and extended exponentially to $||\mathbf{x}|| = 20\,000$ to form a semicircular computational domain with approximately 6 192 elements. The h at the surface is chosen to encapsulate the boundary layer fully at the highest Pe simulated. The boundaries of this mesh are split into four regions: an inlet with Dirichlet boundary conditions on velocity for the incoming flow, an outlet with no stress, the surface of the squirmer with Dirichlet condition using the tangential slip velocity \mathbf{u}^S , and finally the line of symmetry on which the radial component of velocity is set to zero, $u_r = 0$, as a necessary condition of axisymmetric flow. This mesh gives at least four digits of accuracy for drag calculations when compared to the analytic, constant-viscosity Stokes drag on an inert sphere.

To solve the coupled, nonlinear system (14) and (15) numerically using only linear solvers, we employ an iterative splitting scheme: Solve one system, then use that solution as a parameter in the other system, and iterate until convergence is reached. Specifically, the Stokes system (14) is solved first with an initial, constant-viscosity field, and then the resulting velocity field \mathbf{u} is used in solving Eq. (15); when $k_c \neq 0$, an iterative technique to update $H(c)$ is used until convergence of c . The resulting c solution is used to compute the μ field in Eqs. (14) using Eq. (5), then we solve the Stokes system again, etc. A solution $\{\mathbf{u}, p, c\}$ to Eqs. (14) and (15) is considered to reach convergence only when an absolute difference tolerance of 10^{-6} is achieved for all discretized variables at each degree of freedom.

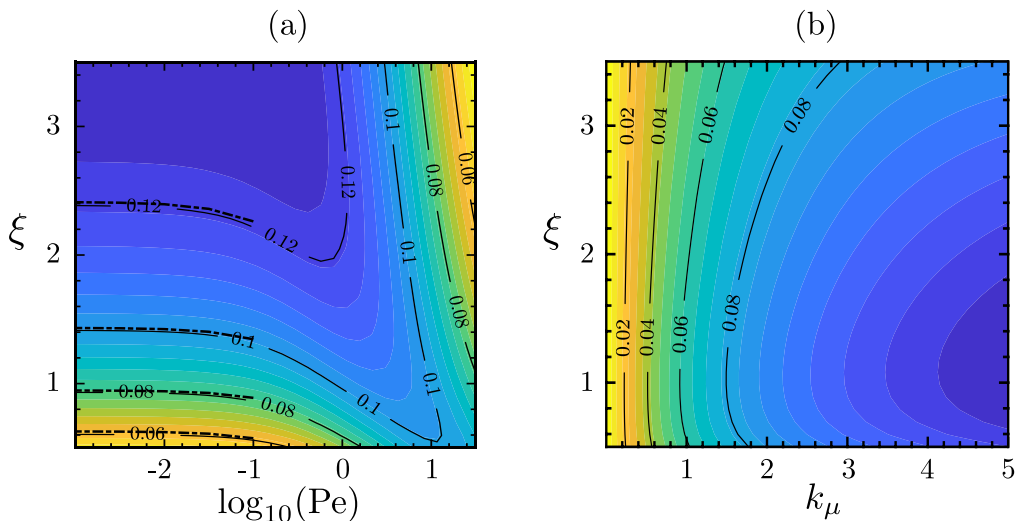


FIG. 3. Asymptotic validation and extension to strong coupling. (a) The first-order velocity improvement U_1 for $k_\mu = 0.001$ is plotted, where $U = U_0 + k_\mu U_1$ ($k_\kappa = 0$). The dash-dotted line represents the low-Pe asymptotic results from Ref. [53]. (b) Extension as k_μ increases to strongly nonlinear regime shows ξ and k_μ dependence of V , as defined in Eq. (16) to represent modification to swimming speed.

III. RESULTS

A squirmer's swimming speed U and nutrient flux Φ depend on whether the squirmer is in a constant- or variable-viscosity fluid. To quantify the relative change in a squirmer's performance, we define two normalized parameters V and J as follows:

$$V = \frac{U - U_0}{U_0}, \quad J = \frac{\Phi - \Phi_0}{\Phi_0}, \quad (16)$$

where U_0 is the free-swimming speed of the squirmer in a corresponding constant-viscosity fluid, and Φ_0 is the analogous quantity for nutrient flux. V represents the velocity modification, and J represents the nutrient flux modification. Parameter regimes with $V > 0$ indicate improvement of swimming performance in the variable-viscosity environment. Regimes with $J > 0$, and c being interpreted as nutrient concentration, correspond to feeding enhancement in the variable-viscosity environment.

In Sec. III A, the effect of nutrient-viscosity coupling on a treadmill squirmer is investigated, specifically by varying Pe , k_μ , k_κ , and ξ ; additionally, changes in power expenditure and hydrodynamic efficiency are addressed. Then in Sec. III B different surface stroke modes and spheroidal geometries are introduced and their influence on the swimming and feeding performance is discussed.

A. Spherical treadmill squirmer

In this section, the swimming and feeding performance of a spherical ‘‘treadmill’’ squirmer ($\beta_1 = \sqrt{3/2}$) is examined. To isolate the effect of k_μ , we temporarily let nutrient diffusivity be constant ($k_\kappa = 0$); we will examine the effect of nonzero k_κ later. The effect of Pe and ξ on velocity and flux modification, V and J , is shown in Fig. 4 for increasing strength of coupling, k_μ . Interestingly, even for very small Pe , the velocity modification is nonzero and increases monotonically with k_μ ; however, V is *not* monotonic in Pe , and experiences an extreme value for $\text{Pe} = O(5)$, although the Pe at which this extreme value occurs decreases with increasing coupling nonlinearity, ξ . In a

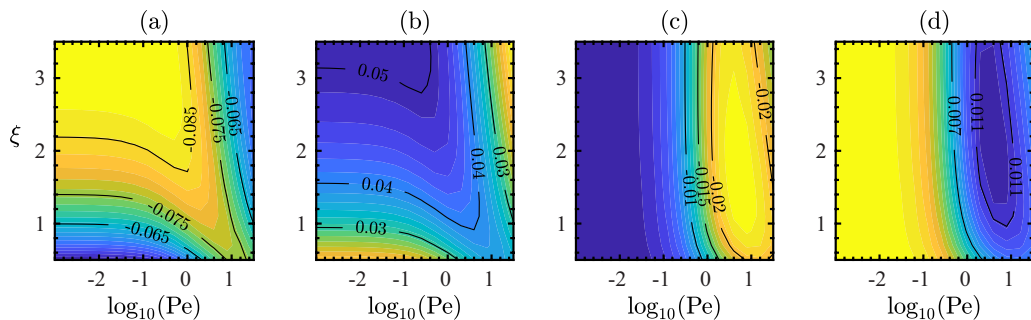


FIG. 4. Effect of Pe and ξ on speed (V) and flux (J) modification. [(a), (b)] V for $k_\mu = -0.5$ and 0.5 and [(c), (d)] J for $k_\mu = -0.5$ and 0.5 , respectively. Both V and J monotonically increase in k_μ . It is found that the nonlinear relationship between viscosity and nutrient concentration does not change the qualitative contours of V or J .

low- Pe environment with constant diffusivity, flux modification, unlike V , is unaffected by variable viscosity. As Pe increases, J also displays nonmonotonic behavior with extreme values observed for $Pe \approx 7$. It is interesting to note that the extreme value of Pe for J is independent of the power coefficient ξ , while the extreme value of V is affected by the value of this power coefficient. In this manner, the nonlinearity of the nutrient-viscosity relationship affects swimming speed, but not nutrient flux.

These observations suggest the following physical explanation: For small Pe , diffusion dominates, and so there is no nutrient boundary layer near the surface of the swimmer. This lack of a boundary layer means that nutrient in the near field is similar in both the constant- and variable-viscosity fluids, meaning the diffusive fluxes across the boundary are similar as well, as we observe. However, the drag on the surface of the squirmer is a *nonlocal* effect, which allows for a modified free-swimming velocity even in the absence of a boundary layer. As Pe increases, the advection effect dominates over diffusion, and a boundary layer develops. This nutrient boundary layer causes asymmetric distribution of the viscosity around the squirmer. At $Pe = O(5)$, the thickness of the boundary layer has maximum effect on propulsion, as there is enough viscosity to “push off” against. As the Pe increases even further, the nutrient boundary layer becomes thinner, and the viscosity of the fluid in the near-field decreases (increases) even further for $k_\mu > 0$ ($k_\mu < 0$). The thickness of the *viscosity* boundary layer, as opposed to the nutrient boundary layer, can be further controlled by the nonlinearity parameter ξ (see Fig. 7). This explains why, when increasing Pe , the optimal swimming modification requires decreasing the nonlinearity parameter ξ . This is because decreasing ξ “extends” the viscosity variation with c , such that there is some relationship between Pe and ξ where the viscosity boundary layer is “optimal” for propulsion.

Because the power expenditure is nonconstant even with the constraint on stroke modes in Eq. (12), it is useful to examine modifications to both power consumption and hydrodynamic efficiency as they depend on Pe and ξ . Analogous to our variables for modifications to speed and nutrient flux, we define

$$\mathcal{P}^* = \frac{\mathcal{P} - \mathcal{P}_0}{\mathcal{P}_0}, \quad \eta^* = \frac{\eta - \eta_0}{\eta_0}, \quad (17)$$

where \mathcal{P}_0 and η_0 are the power and efficiency of a squirmer in the constant-viscosity environment. Note that the modification to efficiency can depend on two quantities: the drag on an inert sphere or the power expenditure by the squirmer in a variable viscosity fluid.

The power and efficiency modifications, \mathcal{P}^* and η^* , are shown in Fig. 5. Power expenditure can vary dramatically between the variable- and constant-viscosity cases, but the contours and sign of power modification are qualitatively similar to those for velocity modification. This suggests

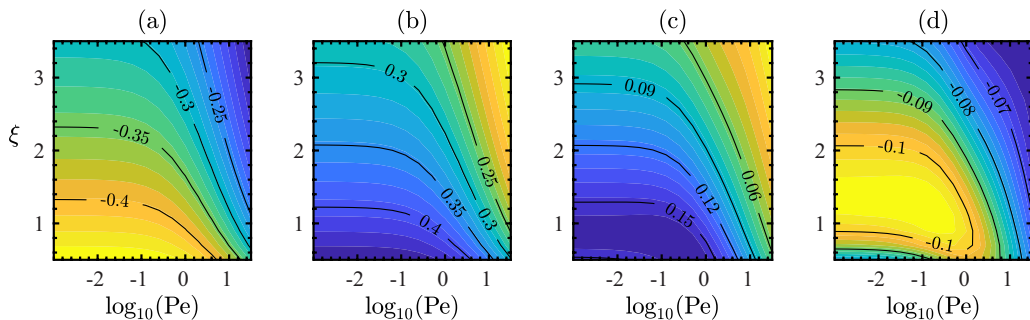


FIG. 5. Effect of Pe and ξ on modification to power (\mathcal{P}^*) and efficiency (η^*). [(a), (b)] Relative power use for $k_\mu = \mp 0.5$ and [(c), (d)] relative low-Re swimming efficiency, as defined in Eq. (17), for $k_\mu \mp 0.5$.

that swimming velocity and power expenditure are both affected in the same manner by the viscosity boundary layer. Additionally, examining the normalized low-Re hydrodynamic efficiency in Figs. 5(c) and 5(d), we see that the nutrient-viscosity relationship completely determines the increase or decrease in efficiency for $k_\mu < 0$ and $k_\mu > 0$, respectively. However, the sign of the efficiency modification has flipped, i.e., environments with negative modification to power have positive modification to efficiency, and vice versa, although the magnitude of the modification is smaller. This is due to the modification to the drag on an inert sphere in a variable-viscosity fluid, not pictured, which does not compensate enough for the changes in power required to move at a prescribed velocity.

Notably, the efficiency in Fig. 5(d) experiences a minimum at small Pe and $\xi \approx 1.5$, which is surprisingly similar to the $\xi = 1.35$ estimated from experimental data on the variation in viscosity with water temperature, as given in Fig. 1. These results suggest that extreme care should be taken when estimating required power for microrobots, particularly those in $k_\mu > 0$ fluids such as thermophoretic microrobots; efficiency estimated from the ambient fluid viscosity will *underestimate* the power required to move at the expected velocity.

Figures 6(a) and 6(b) show the contour plots of nutrient and pressure fields of a treadmill squirmer at small and large Pe , respectively. The top half of each panel contains the nutrient field and flow streamlines and the bottom panel shows the pressure field. Even though nutrient exhibits large changes with increasing Pe , the flow streamlines are largely unaffected. The pressure field, on the other hand, changes dramatically as Pe increases. For small Pe , the pressure is approximately symmetric about the sphere. As Pe increases, however, the viscosity boundary layer develops, and the total pressure difference between the front and back of the swimmer increases as well. This is the most notable observed change in the flow variables compared to the constant-viscosity squirmer, where pressure is unaffected by Pe . Because the streamlines are approximately similar for different Pe , but pressure changes greatly, we hypothesize that viscosity gradients modify the pressure field but only induces small changes in the velocity field.

The pressure field is also found to be affected by k_μ , as predicted by Eq. (7). Although not shown in Fig. 6, the sign of the pressure field switches with the sign of k_μ . Additionally, the pressure difference across the surface from front to back of the squirmer monotonically increases with $|k_\mu|$. Because swimming performance is also monotonic in k_μ , we conclude that the enhancement of the swimming performance due to variable viscosity occurs when the pressure force is in the *same direction* of swimming motion. By a similar argument, when the pressure force is in the opposite direction of the swimming, performance is hindered. This effect modifies the free-swimming speed through nonlocal interactions affecting the drag on the body.

In Fig. 7, two representative cases for the viscosity field μ for different ξ are shown. We immediately notice that the streamlines are approximately the same with minor changes near the body. Although not shown here, the increasing swimming modification is paired with an increase in

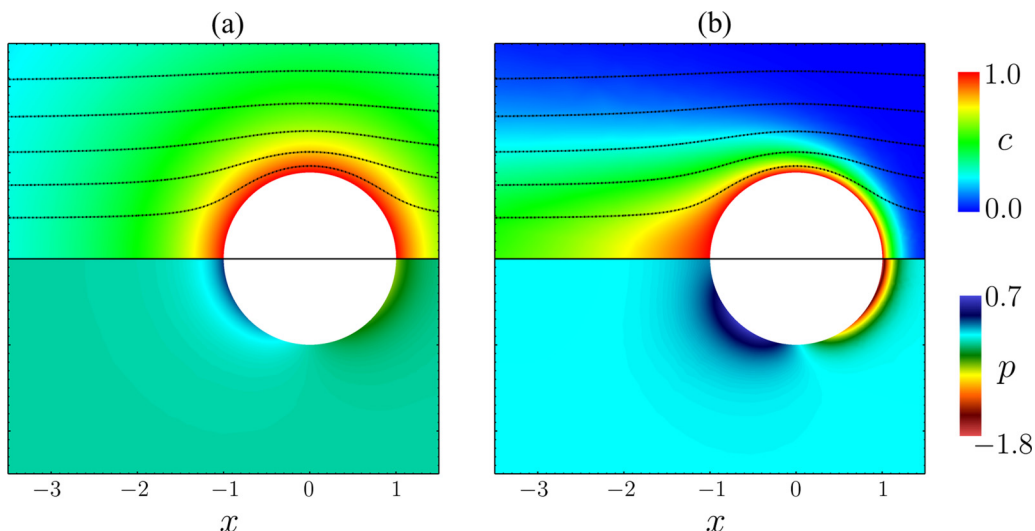


FIG. 6. Effect of Pe on a treadmill squirmer with $\xi = 1.0$ and $k_\mu = 0.5$; nutrient field with streamlines on top and pressure field on bottom. (a) $Pe = 0.01$, both nutrient and pressure are symmetric due to the diffusion-dominated regime. (b) $Pe = 10$, advection-dominated regime causes an asymmetry in pressure and nutrient fields which results in larger modifications to swimming speed and nutrient flux.

the asymmetrical pattern and magnitude of the pressure field, as explained previously. This indicates the advantage of using a power-law model, Eq. (5), as a canonical form to represent the relation between the nutrient and viscosity: By changing ξ , one can change the width of the viscosity boundary layer near the surface of the squirmer, which in turn affects modifications to swimming speed and nutrient flux.

The previous analyses are extended to situations in which both viscosity and diffusivity vary simultaneously. This assumption is more physically realistic due to the Stokes-Einstein relationship between bulk viscosity and diffusivity. In Fig. 8, we examine changes in V for low- and high- Pe environments as the coefficient of nonlinearity ξ and the ratio k_κ/k_μ are varied; specifically, k_μ is kept fixed and k_κ is varied. The expected physical scenario is $k_{\text{ratio}} < 0$, but ratios between -1 and 1 were examined for completeness. First, note that the line corresponding to $k_{\text{ratio}} = 0$ simply gives the results for constant diffusivity cases as discussed in the previous section. By increase or decrease of k_κ , we see that the overall effect on velocity modification is minimal. However, these

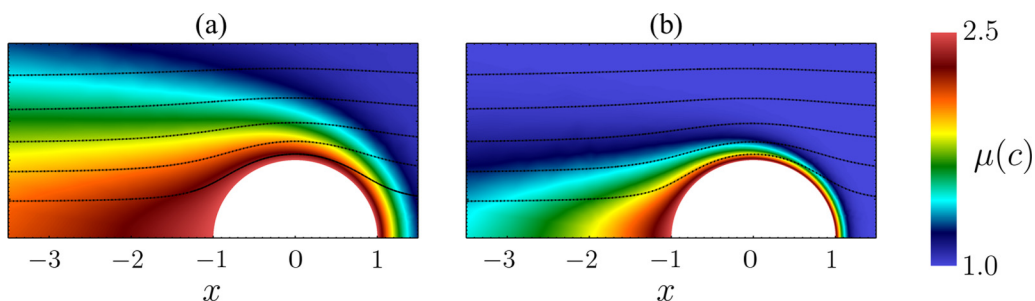


FIG. 7. Viscosity fields for two ξ ($k > 0$): (a) $\xi = 0.5$, (b) $\xi = 2.0$. The nutrient boundary layer is similar in both regimes ($Pe = 10$); changing ξ affects the viscosity field which determines the thickness of the viscosity boundary layer, which in turn affects the swimming and feeding performances.

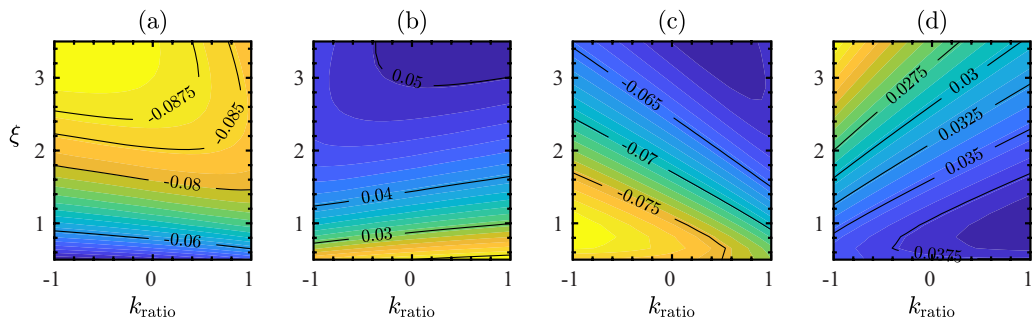


FIG. 8. Effect of k_{ratio} and ξ on modification to swimming speed V . [(a), (b)] $k_{\mu} = \mp 0.5$ at $\text{Pe} = 0.1$ and [(c), (d)] $k_{\mu} = \mp 0.5$ at $\text{Pe} = 10$. Velocity changes, while quantitatively different as Pe increases, also depends on the value of k_{μ} .

minimal effects on velocity modification are contrasted sharply with the strong changes in nutrient flux modification, as presented in Fig. 9. The physical explanation for the effect of changing k_{ratio} are explained using Fig. 10, but for concreteness we focus on the case of $k_{\mu} > 0$, $k_{\kappa} < 0$ [e.g., the left half of Figs. 9(b) and 9(c)] to physically explain the drastic change in nutrient flux modification. In this regime, regardless of Pe , the negative diffusivity strength indicates that the nutrient diffuses faster near the swimmer and as a result the nutrient boundary layer shrinks compared to the $k_{\kappa} = 0$ case. This sharper boundary layer means the normal derivative of nutrient at the boundary is higher, and therefore the nutrient flux increases significantly, even for $\text{Pe} \approx 0$.

The results of this section suggest that k_{μ} primarily affects velocity through modifications to the nonlocal drag force while having minimal effect on the nutrient flux modification. In contrast, k_{κ} significantly influences the nutrient flux modification with minor effect on swimming speed modifications. Now that we have established these heuristics for the spherical, treadmill squirmer, in the next section the influence of mixing modes and geometry on swimming and nutrient flux modification will be discussed.

B. Spheroidal squirmers with coupled stroke modes

Now that we have gained intuition for how variable viscosity and diffusivity affects spherical treadmill squirmers, we examine how the combination of different surface modes affects the swimming and feeding performance of spheroidal squirmers. Following previous studies, we only consider the first two modes of surface motion because the first two modes have a dominant

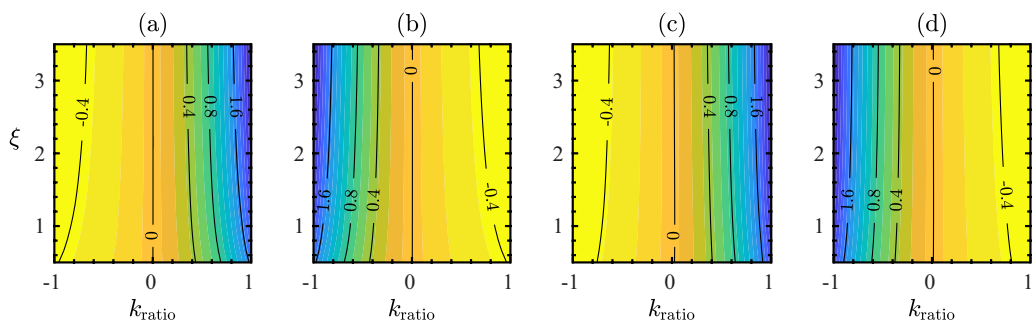


FIG. 9. Effect of k_{ratio} and ξ on modification to nutrient flux J . [(a), (b)] $k_{\mu} = \mp 0.5$ at $\text{Pe} = 0.1$ and [(c), (d)] $k_{\mu} = \mp 0.5$ at $\text{Pe} = 10$. While for $k_{\text{ratio}} = 0$ nutrient flux modification is minimal, the modification is drastic as the diffusivity is allowed to vary proportionally to the viscosity variation.

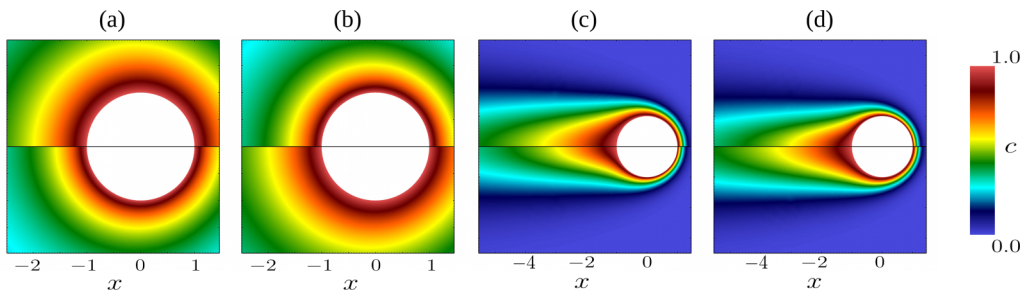


FIG. 10. Effect of k_{ratio} on nutrient boundary layer. Parameters match those of Figs. 8 and 9. For each parameter regime, the nutrient field for $k_{\text{ratio}} = -1$ (top) or $k_{\text{ratio}} = 1$ (bottom) and $\xi = 2$ is shown. Changing k_{ratio} affects the nutrient boundary layer, which has a significant effect on the nutrient flux.

role in squirmer performance [41,53,57,58]. Combinations of the first (treadmill) and the second (pusher-puller) mode are examined; in a constant-viscosity fluid, propulsion is entirely generated by the first mode while the second mode only mixes the fluid and provides zero net thrust. In the case of nutrient-dependent viscosity, this mixing changes the local viscosity of the fluid, and therefore the second mode *can* affect the swimming speed of the squirmer. To fix the effect of diffusivity, in this section we fix $k_{\text{ratio}} = -1$ or, equivalently, $k_{\kappa} = -k_{\mu}$.

In Fig. 11(a), we see an interesting asymmetry in speed modification when $\beta_2/\beta_1 > 0$ (puller-like) versus when $\beta_2/\beta_1 < 0$ (pusher-like), as opposed to flux modification in Fig. 11(b), which is approximately symmetric in β_2/β_1 . For small Pe, all mode combinations have the same effect, giving a small boost in swimming speed. Increasing the effect of advection (Pe = 1), there is an equal contribution of advection and diffusion and pusher-like squirmers experience more of a boost than puller-like squirmers, although for all stroke modes a positive modification to swimming is observed. Nutrient uptake, however, shows a maximum near treadmill squirmers ($\beta_2/\beta_1 = 0$), indicating that the feeding is optimized for the first mode. As Pe is increased even further, and advection dominates, the effect of mixing from β_2 has an adverse effect on swimming modification for some squirmers ($\beta_2/\beta_1 \gtrsim 1$ and $\beta_2/\beta_1 \lesssim 3$) while nutrient flux experiences a higher modification for these mixing-dominated stroke modes. To summarize, the effect of stroke mode becomes more prevalent as Pe increases; in particular, the swimming speed increase is

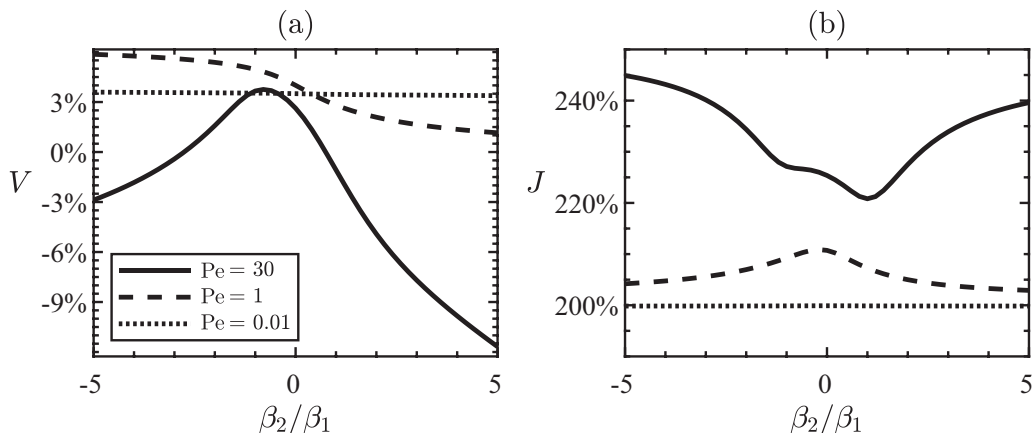


FIG. 11. Effect of β_2/β_1 ratio on V and J for diffusion-dominated (Pe = 0.01, dots), balanced (Pe = 1, dash), and advection-dominated (Pe = 30, solid) regimes. Speed modification (V) is asymmetric with respect to stroke mode, while J is approximately symmetric in β_2/β_1 and increases monotonically with Pe.

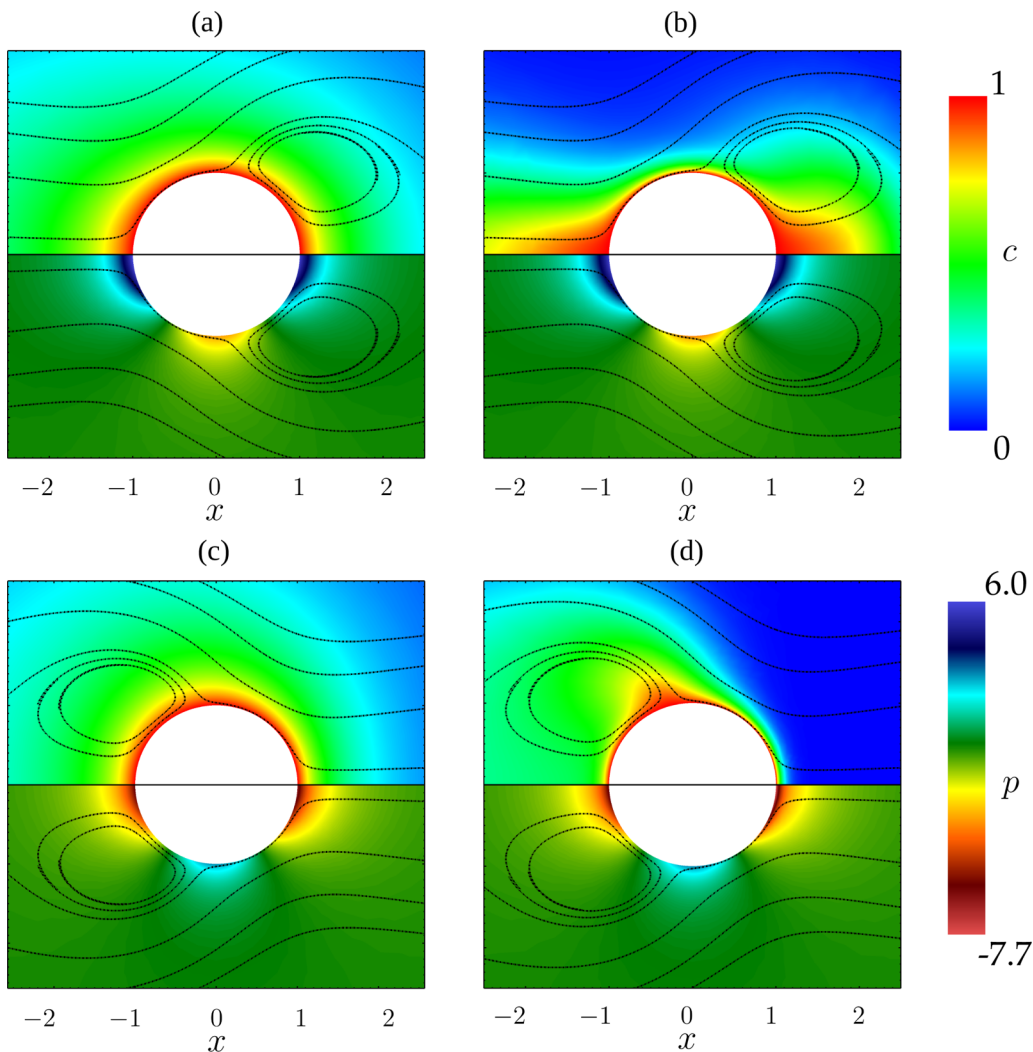


FIG. 12. Effect of stroke mode on nutrient and pressure fields. Top (bottom) half of panels corresponds to nutrient c (pressure p). Left panels [(a), (c)] correspond to balanced regimes ($Pe = 1$) whereas right panels [(b), (d)] correspond to advection-dominated regimes ($Pe = 20$). Top panels [(a), (b)] are pusher-like squirmers ($\beta_2/\beta_1 = -3$); bottom panels [(c), (d)] are puller-like ($\beta_2/\beta_1 = 3$). As all squirmers are swimming in the same direction, the placement of the stagnation point either helps or hinders locomotion, but does not affect the nutrient flux modification.

dependent on whether the squirmer is puller-like or pusher-like, whereas the effect of stroke mode on nutrient flux is symmetric with respect to β_2/β_1 . We should note that the overall increase in nutrient flux modification values is due to the nonzero k_c .

The nutrient and pressure fields for four different β_2/β_1 - Pe combinations are shown in Fig. 12. Figures 12(a) and 12(b) show $\beta_2/\beta_1 < 0$ (pusher-like) for small and large Pe , respectively. The stagnation point on the surface is slightly shifted to the right of the center line, and a stagnation point in the flow induces some circulation on the right side of the squirmer. These stagnation points are reversed in the case of $\beta_2/\beta_1 > 0$ (puller-like), as shown in Figs. 12(c) and 12(d). All swimmers have positive velocity, so pusher-like squirmers induce a stagnation point in front of their bodies

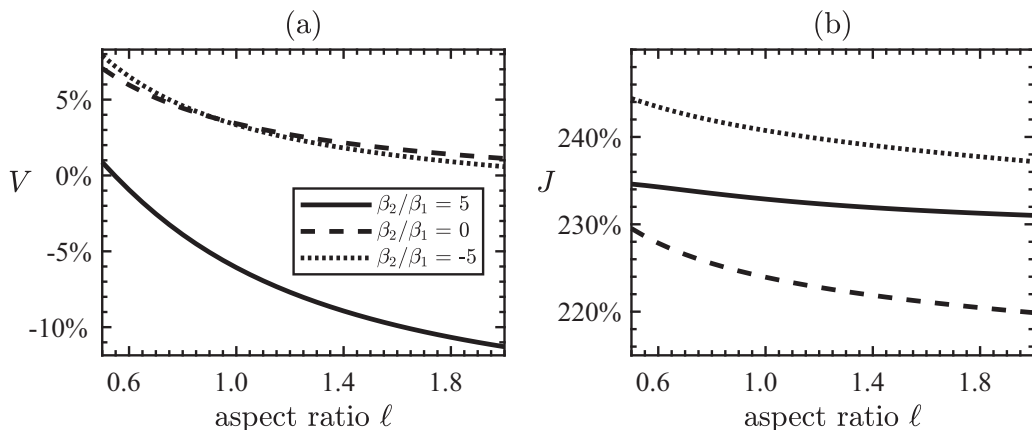


FIG. 13. Effect of shape. Oblate spheroids experience larger increases in speed and flux modifications than prolate spheroids, although the stroke mode dependence largely mirrors the results for spheres.

while puller-like squirmers induce a stagnation point behind their bodies. Comparing the high-Pe Figs. 12(b) and 12(d), we see that the boundary layer is thin at different places: thin on top for pusher-like and thin on sides for puller-like squirmers. This nutrient boundary layer in turn creates a viscosity boundary layer, which as we have explained previously affects the performance of the swimmer.

We now expand our discussion beyond spheres to spheroidal squirmers. As mentioned previously, the surface area is kept constant in order to isolate the effect of geometry on speed and flux modification. We present the results for different aspect ratio ℓ of the spheroid at fixed $Pe = 10$, for three representative β_2/β_1 ratios selected based on results above for stroke mode coupling. As shown in Fig. 13, for all three stroke mode combinations, both speed and flux modifications monotonically decrease in ℓ , meaning that oblate spheroids have more positive changes in swimming and feeding due to spatially varying viscosity than prolate spheroids of the same surface area. Additionally, there is an asymmetry in the stroke mode coupling. In Fig. 13(a), the speed modification V is positive but decreases to zero as ℓ increases for pusher-like and treadmill squirmers ($\beta_2/\beta_1 \leq 0$), while for puller-like squirmers ($\beta_2/\beta_1 > 0$), speed modification is negative for all but the most

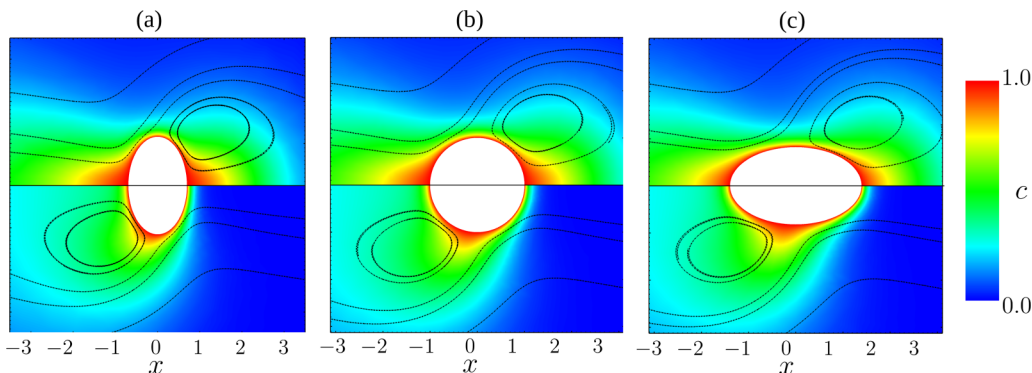


FIG. 14. Effect of shape on nutrient field. Top panels show pusher-like squirmers ($\beta_2/\beta_1 = -5$), and the bottom panels show puller-like squirmers ($\beta_2/\beta_1 = 5$) for various aspect ratios: (a) $\ell = 0.6$, (b) $\ell = 1.0$, and (c) $\ell = 1.7$. The effect of stroke mode for different geometries is qualitatively similar to a sphere, suggesting shape is only a minor effect.

oblate spheroids simulated. In Fig. 11(b), nutrient flux modification is positive, although it decreases monotonically in ℓ , for all stroke mode combinations. Treadmill squirmers ($\beta_2/\beta_1 = 0$) experience the lowest flux modification, although it is still positive, reinforcing the result in Fig. 11(b). To summarize, the qualitative results for the effect of shape largely mirror the results for spheres, with the minor addition that oblate spheroids experience more positive modification in speed and flux than prolate spheroids.

Figure 14 shows three representative spheroids along with their nutrient field and streamlines for two different surface actuation of pusher-like (top panels) and puller-like (bottom panels). All squirmers have positive velocity. Similar to spherical squirmers, the stagnation point in front of the squirmer leads to improved swimming performance over the constant-viscosity case, while the stagnation point behind the squirmer has a negative effect on swimming modification. The flow profiles are qualitatively similar for all ℓ , indicating that shape is only a minor effect to consider when evaluating the performance change due to the presence of viscosity gradients.

IV. CONCLUSIONS

In this paper, we extended previous asymptotic results, where analysis was restricted to examining the effect of a weak coupling between viscosity and nutrient on swimming performance for a spherical squirmer [53]. The numerical method employed here allows us to extend these previous results by considering modifications to nutrient flux, power, and hydrodynamic efficiency, in addition to swimming speed for spheroidal swimmers, not just spheres. These quantities of interest were studied by examining the effects of the relative strength of advection to diffusion (represented through Pe), the type of nutrient-viscosity relationship (through k_μ and ξ), nutrient-dependent diffusivity (through k_κ), the stroke mode coupling (through β_2/β_1), and the shape of the spheroid (through aspect ratio ℓ). We observed that all of the above parameters affected the swimming speed of the squirmer and the nutrient flux at its boundary, although some were more influential than others.

We now summarize heuristics that can be taken from our main results. We found that (1) variable viscosity primarily affected swimming speed while variable diffusivity primarily affected the nutrient flux, (2) the swimming speed modification is primarily generated by changes in the pressure field as opposed to the velocity field, (3) pusher-like and puller-like squirmers experienced equivalent boosts in nutrient acquisition, while pusher-like squirmers obtained more positive velocity modification than puller-like squirmers, and (4) the aspect ratio of the squirmer was not found to significantly affect the results, meaning that future studies can reliably capture phenomena of interest using only spherical squirmers. An interesting result related to the design of microswimmers is that, in the case of swimming in a fluid with temperature-dependent viscosity, the power required to swim at an expected velocity will be *underestimated* if one assumes the fluid has constant viscosity. Therefore, care should be taken when designing swimmers which can affect a fluid's local rheology. These power results should be extended to biological swimmers with caution, as the power expenditure from time-dependent motion [79] and fully resolved cilia dynamics [80] show that the steady squirmer model drastically underestimates power consumption of actual biological swimmers. All of these results were only achievable once the fully nonlinear system was solved using a numerical method and demonstrate that the asymptotic analysis previously employed, while elegant, can only capture the physics of a weakly coupled system and is not able to reveal the physics of the system with strong interaction between the feeding and swimming.

In conclusion, we presented how several quantities of interest related to microswimmer locomotion change in a fluid with nutrient-dependent viscosity. The relatively insignificant change in velocity profile, coupled with the significant changes in pressure distribution due to the presence of viscosity gradients, warrants future study. An additional extension would be investigation into the possibility of purely mixing modes (β_n , $n \geq 2$) enabling locomotion that is otherwise impossible in constant-viscosity fluids as has been observed in other non-Newtonian fluids. Finally, including biological unsteadiness by employing the unsteady Stokes equation as well as

alternative interpretations of the Peclét number—e.g., using reorientation times due to biological or thermal noise to investigate how variable viscosity affect chemotaxis behavior in groups of microswimmers—would be interesting. These results have implications for designing the next generation of artificial microswimmers, and in particular demonstrated the promise of using a feedback mechanism between passive and active modes of motion.

ACKNOWLEDGMENTS

P.S.E. is supported by the National Science Foundation (NSF) Graduate Research Fellowship under Grant No. 1449440. K.S. is partially supported by Florida State University Research Fund and is supported by NSF EFRI C3 Soft Robotics under Grant No. 1935278. The resources and support of the FSU Research Computing Center are gratefully acknowledged.

- [1] S. Cho, S. J. Park, S. Y. Ko, J.-O. Park, and S. Park, Development of bacteria-based microrobot using biocompatible poly (ethylene glycol), *Biomed. Microdevices* **14**, 1019 (2012).
- [2] O. Schauer, B. Mostaghaci, R. Colin, D. Hürtgen, D. Kraus, M. Sitti, and V. Sourjik, Motility and chemotaxis of bacteria-driven microswimmers fabricated using antigen 43-mediated biotin display, *Sci. Rep.* **8**, 9801 (2018).
- [3] S. Zheng, J. Han, S. Cho, V. D. Nguyen, S. Y. Ko, J.-O. Park, and S. Park, Motility steering of bacteriobots using chemical gradient microchannel, in *2016 6th IEEE International Conference on Biomedical Robotics and Biomechatronics (BioRob)* (IEEE, UTown, Singapore, 2016), pp. 140–144.
- [4] J. Zhuang, B.-W. Park, and M. Sitti, Propulsion and chemotaxis in bacteria-driven microswimmers, *Adv. Sci.* **4**, 1700109 (2017).
- [5] B. J. Nelson, I. K. Kaliakatsos, and J. J. Abbott, Microrobots for minimally invasive medicine, *Annu. Rev. Biomed. Eng.* **12**, 55 (2010).
- [6] K. E. Peyer, L. Zhang, and B. J. Nelson, Bio-inspired magnetic swimming microrobots for biomedical applications, *Nanoscale* **5**, 1259 (2013).
- [7] I. S. Aranson, Swimmers by design, *Nature (London)* **531**, 312 (2016).
- [8] J. Feng and S. K. Cho, Mini and micropropulsion for medical swimmers, *Micromachines* **5**, 97 (2014).
- [9] A. Ghanbari and M. Bahrami, A novel swimming microrobot based on artificial cilia for biomedical applications, *J. Intel. Robot. Syst.* **63**, 399 (2011).
- [10] H-W. Huang, F. E. Uslu, P. Katsamba, E. Lauga, M. S. Sakar, and B. J. Nelson, Adaptive locomotion of artificial microswimmers, *Sci. Adv.* **5**, eaau1532 (2019).
- [11] S. Kim, S. Lee, J. Lee, B. J. Nelson, L. Zhang, and H. Choi, Fabrication and manipulation of ciliary microrobots with non-reciprocal magnetic actuation, *Sci. Rep.* **6**, 30713 (2016)
- [12] J. Li, B. Esteban-Fernández de Ávila, W. Gao, L. Zhang, and J. Wang, Micro/nanorobots for biomedicine: Delivery, surgery, sensing, and detoxification, *Sci. Robot.* **2**, eaam6431 (2017).
- [13] S. Palagi, E. W. H. Jager, B. Mazzolai, and L. Beccai, Propulsion of swimming microrobots inspired by metachronal waves in ciliates: From biology to material specifications, *Bioinspiration Biomimetics* **8**, 046004 (2013).
- [14] Y. Hatwalne, S. Ramaswamy, M. Rao, and R. Aditi Simha, Rheology of Active-Particle Suspensions, *Phys. Rev. Lett.* **92**, 118101 (2004).
- [15] S. Rafañ, L. Jibuti, and P. Peyla, Effective Viscosity of Microswimmer Suspensions, *Phys. Rev. Lett.* **104**, 098102 (2010).
- [16] A. Sokolov and I. S. Aranson, Reduction of Viscosity in Suspension of Swimming Bacteria, *Phys. Rev. Lett.* **103**, 148101 (2009).
- [17] C. Datt and G. J. Elfring, Active Particles in Viscosity Gradients, *Phys. Rev. Lett.* **123**, 158006 (2019).
- [18] B. Liebchen, P. Monderkamp, B. ten Hagen, and H. Löwen, Viscotaxis: Microswimmer Navigation in Viscosity Gradients, *Phys. Rev. Lett.* **120**, 208002 (2018).

- [19] D. A. Gagnon and P. E. Arratia, The cost of swimming in generalized Newtonian fluids: Experiments with *C. elegans*, *J. Fluid Mech.* **800**, 753 (2016).
- [20] J. Sznitman and P. E. Arratia, *Locomotion through Complex Fluids: An Experimental View* (Springer, New York, 2015), pp. 245–281.
- [21] J. P. Celli, B. S. Turner, N. H. Afdhal, S. Keates, I. Ghiran, C. P. Kelly, R. H. Ewoldt, G. H. McKinley, P. So, S. Erramilli *et al.*, *Helicobacter pylori* moves through mucus by reducing mucin viscoelasticity, *Proc. Natl. Acad. Sci. USA* **106**, 14321 (2009).
- [22] K. M. Ottemann and A. C. Lowenthal, *Helicobacter pylori* uses motility for initial colonization and to attain robust infection, *Infect. Immun.* **70**, 1984 (2002).
- [23] M. J. Daniels, J. M. Longland, and J. Gilbert, Aspects of motility and chemotaxis in spiroplasmas, *Microbiology* **118**, 429 (1980).
- [24] K. Takabe, H. Tahara, M. S. Islam, S. Affroze, S. Kudo, and S. Nakamura, Viscosity-dependent variations in the cell shape and swimming manner of leptospira, *Microbiology* **163**, 153 (2017).
- [25] R. E. Goldstein, Green algae as model organisms for biological fluid dynamics, *Annu. Rev. Fluid Mech.* **47**, 343 (2015).
- [26] M. B. Short, C. A. Solari, S. Ganguly, T. R. Powers, J. O. Kessler, and R. E. Goldstein, Flows driven by flagella of multicellular organisms enhance long-range molecular transport, *Proc. Natl. Acad. Sci. USA* **103**, 8315 (2006).
- [27] C. A. Solari, S. Ganguly, J. O. Kessler, R. E. Michod, and R. E. Goldstein, Multicellularity and the functional interdependence of motility and molecular transport, *Proc. Natl. Acad. Sci. USA* **103**, 1353 (2006).
- [28] H. Kurtuldu, J. S. Guasto, K. A. Johnson, and J. P. Gollub, Enhancement of biomixing by swimming algal cells in two-dimensional films, *Proc. Natl. Acad. Sci. USA* **108**, 10391 (2011).
- [29] I. M. Zaid, J. Dunkel, and J. M. Yeomans, Lévy fluctuations and mixing in dilute suspensions of algae and bacteria, *J. R. Soc., Interface* **8**, 1314 (2011).
- [30] R. R. Bennett and R. Golestanian, A steering mechanism for phototaxis in chlamydomonas, *J. R. Soc., Interface* **12**, 20141164 (2015).
- [31] H. J. Hoops, M. C. Brighton, S. M. Stickles, and P. R. Clement, A test of two possible mechanisms for phototactic steering in *Volvox carteri* (chlorophyceae), *J. Phycol.* **35**, 539 (1999).
- [32] M. Morse, A. Huang, G. Li, M. R. Maxey, and J. X. Tang, Molecular adsorption steers bacterial swimming at the air/water interface, *Biophys. J.* **105**, 21 (2013).
- [33] J. L. Anderson, Colloid transport by interfacial forces, *Annu. Rev. Fluid Mech.* **21**, 61 (1989).
- [34] R. Golestanian, T. B. Liverpool, and A. Ajdari, Designing phoretic micro- and nano-swimmers, *New J. Phys.* **9**, 126 (2007).
- [35] S. Michelin and E. Lauga, Geometric tuning of self-propulsion for Janus catalytic particles, *Sci. Rep.* **7**, 42264 (2017).
- [36] J. R. Blake, A spherical envelope approach to ciliary propulsion, *J. Fluid Mech.* **46**, 199 (1971).
- [37] E. Lauga and R. E. Goldstein, Dance of the microswimmers, *Phys. Today* **65**, 30 (2012).
- [38] M. J. Lighthill, On the squirming motion of nearly spherical deformable bodies through liquids at very small Reynolds numbers, *Commun. Pure Appl. Math.* **5**, 109 (1952).
- [39] H. Nganguia and O. S. Pak, Squirming motion in a Brinkman medium, *J. Fluid Mech.* **855**, 554 (2018).
- [40] O. S. Pak and E. Lauga, Generalized squirming motion of a sphere, *J. Eng. Math.* **88**, 1 (2014).
- [41] T. J. Pedley, Spherical squirmers: Models for swimming micro-organisms, *IMA J. Appl. Math.* **81**, 488 (2016).
- [42] A. E. Patteson, A. Gopinath, and P. E. Arratia, Active colloids in complex fluids, *Curr. Opin. Colloid Interface Sci.* **21**, 86 (2016).
- [43] J. Happel and H. Brenner, *Low Reynolds Number Hydrodynamics: With Special Applications to Particulate Media*, 2nd ed. (Noordhoff, 1973).
- [44] G. J. Elfring, A note on the reciprocal theorem for the swimming of simple bodies, *Phys. Fluids* **27**, 023101 (2015).
- [45] C. Pozrikidis, Reciprocal identities and integral formulations for diffusive scalar transport and Stokes flow with position-dependent diffusivity or viscosity, *J. Eng. Math.* **96**, 95 (2016).

- [46] H. A. Stone and A. D. T. Samuel, Propulsion of Microorganisms by Surface Distortions, *Phys. Rev. Lett.* **77**, 4102 (1996).
- [47] C. Datt, L. Zhu, G. J. Elfring, and O. S. Pak, Squirming through shear-thinning fluids, *J. Fluid Mech.* **784**, R1 (2015).
- [48] H. Nganguia, K. Pietrzyk, and O. S. Pak, Swimming efficiency in a shear-thinning fluid, *Phys. Rev. E* **96**, 062606 (2017).
- [49] C. Datt, G. Natale, S. G. Hatzikiriakos, and G. J. Elfring, An active particle in a complex fluid, *J. Fluid Mech.* **823**, 675 (2017).
- [50] M. De Corato, F. Greco, and P. L. Maffettone, Locomotion of a microorganism in weakly viscoelastic liquids, *Phys. Rev. E* **92**, 053008 (2015).
- [51] M. De Corato, F. Greco, and P. L. Maffettone, Reply to “Comment on ‘Locomotion of a microorganism in weakly viscoelastic liquids,’” *Phys. Rev. E* **94**, 057102 (2016).
- [52] G. Natale, C. Datt, S. G. Hatzikiriakos, and G. J. Elfring, Autophoretic locomotion in weakly viscoelastic fluids at finite Péclet number, *Phys. Fluids* **29**, 123102 (2017).
- [53] K. Shoole and P. S. Eastham, Effects of nonuniform viscosity on ciliary locomotion, *Phys. Rev. Fluids* **3**, 043101 (2018).
- [54] J. C. Strikwerda, *Finite Difference Schemes and Partial Differential Equations*, Vol. 88 (SIAM, Philadelphia, 2004).
- [55] C. Pozrikidis, *Boundary Integral and Singularity Methods for Linearized Viscous Flow* (Cambridge University Press, Cambridge, UK, 1992).
- [56] D. J. Smith, A boundary element regularized Stokeslet method applied to cilia- and flagella-driven flow, *Proc. R. Soc. London, Ser. A* **465**, 3605 (2009).
- [57] V. Magar, T. Goto, and T. J. Pedley, Nutrient uptake by a self-propelled steady squirmer, *Q. J. Mech. Appl. Math.* **56**, 65 (2003).
- [58] S. Michelin and E. Lauga, Optimal feeding is optimal swimming for all Péclet numbers, *Phys. Fluids* **23**, 101901 (2011).
- [59] V. Lobaskin and B. Dünweg, A new model for simulating colloidal dynamics, *New J. Phys.* **6**, 54 (2004).
- [60] A. W. Islam and E. S. Carlson, Viscosity models and effects of dissolved CO₂, *Energy Fuels* **26**, 5330 (2012).
- [61] Z. Kodejš, I. Sláma, and J. Novák, Viscosity of the concentrated aqueous solutions of calcium chloride and nitrate, *Chem. Papers* **30**, 439 (1976).
- [62] M. McBride-Wright, G. C. Maitland, and J. P. M. Trusler, Viscosity and density of aqueous solutions of carbon dioxide at temperatures from (274 to 449) K and at pressures up to 100 Mpa, *J. Chem. Eng. Data* **60**, 171 (2014).
- [63] U. P. Strauss and E. H. Smith, Polyphosphates as polyelectrolytes. II. Viscosity of aqueous solutions of Graham’s salts, *J. Am. Chem. Soc.* **75**, 6186 (1953).
- [64] V. R. N. Telis, J. Telis-Romero, H. B. Mazzotti, and A. L. Gabas, Viscosity of aqueous carbohydrate solutions at different temperatures and concentrations, *Int. J. Food Prop.* **10**, 185 (2007).
- [65] H. Winet, Ciliary propulsion of objects in tubes: Wall drag on swimming tetrahymena (ciliata) in the presence of mucin and other long-chain polymers, *J. Exp. Biol.* **64**, 283 (1976).
- [66] M. O. McLinden, D. G. Friend, and E. W. Lemmon, Thermophysical properties of fluid systems, in *NIST Chemistry WebBook, NIST Standard Reference Database* (NIST, Gaithersburg, MD, 19980, Vol. 69).
- [67] S. R. Keller and T. Y. Wu, A porous prolate-spheroidal model for ciliated micro-organisms, *J. Fluid Mech.* **80**, 259 (1977).
- [68] K. D. Young, The selective value of bacterial shape, *Microbiol. Mol. Biol. Rev.* **70**, 660 (2006).
- [69] K. Thomsen, Surface area of an ellipsoid, <http://www.numericana.com/answer/ellipsoid.htm#spheroid>.
- [70] S. Michelin and E. Lauga, Efficiency optimization and symmetry breaking in a model of ciliary locomotion, *Phys. Fluids* **22**, 111901 (2010).
- [71] H. C. Elman, D. J. Silvester, and A. J. Wathen, *Finite Elements and Fast Iterative Solvers: With Applications in Incompressible Fluid Dynamics*, Numerical Mathematics and Scientific Computation (Oxford University Press, New York, 2005).

- [72] C. Johnson, *Numerical Solution of Partial Differential Equations by the Finite Element Method* (Dover Publishing, Inc, New York, 2009).
- [73] J. Bezanson, A. Edelman, S. Karpinski, and V. B. Shah, JULIA: A fresh approach to numerical computing, *SIAM Rev.* **59**, 65 (2017).
- [74] P. S. Eastham, eFEMpart, <https://github.com/pseastham/eFEMpart>.
- [75] C. Geuzaine and J.-F. Remacle, Gmsh: A 3-d finite element mesh generator with built-in pre- and post-processing facilities, *Int. J. Num. Methods Engin.* **79**, 1309 (2009).
- [76] H. Childs, E. Brugger, B. Whitlock, J. Meredith, S. Ahern, D. Pugmire, K. Biagas, M. Miller, C. Harrison, G. H. Weber, H. Krishnan, T. Fogal, A. Sanderson, C. Garth, E. W. Bethel, D. Camp, O. Rübel, M. Durant, J. M. Favre, and P. Navrátil, VISIT: An End-User Tool for Visualizing and Analyzing Very Large Data, in *High Performance Visualization—Enabling Extreme Scale Scientific Insight*, CRC Computational Science series (Taylor and Francis, 2012), Chap. 16.
- [77] MATLAB, 9.7.0.1190202 (R2019b) (MathWorks, Natick, MA, 2018).
- [78] M. Tabata, Finite element analysis of axisymmetric flow problems and its application, *Departmental Bulletin Paper* **951**, 69 (1996).
- [79] J. S. Guasto, K. A. Johnson, and J. P. Gollub, Oscillatory Flows Induced by Microorganisms Swimming in Two Dimensions, *Phys. Rev. Lett.* **105**, 168102 (2010).
- [80] H. Ito, T. Omori, and T. Ishikawa, Swimming mediated by ciliary beating: Comparison with a squirmer model, *J. Fluid Mech.* **874**, 774 (2019).